Carbon-13 Nuclear Overhauser Effect and Molecular Motion in Bulk Elastomers

J. Denault and J. Prud'homme*

Department of Chemistry, University of Montreal, Montreal, Quebec, Canada H3C 3V1.
Received April 27, 1988

ABSTRACT: ^{13}C NMR spin–lattice relaxation times, T_1, and nuclear Overhauser enhancement factors, NOEF, have been measured at two Larmor frequencies (20.1 and 100.6 MHz) and over a range of temperature for bulk monodisperse polyisoprene samples ($M_n = 7 \times 10^3$ and 1.3×10^5) having T_g of −67 and −63 °C, respectively. According to the methylene T_1 data analysis made with both the correlation time distribution approach and the Jones–Stockmayer three-bond jump model, a change of regime is observed near 60 °C for the backbone motion. The transition is inferred from singularities in the Arrhenius plots of the average correlation times for segmental motion and in plots of either the distribution width or the kinetic segment length for orientational correlation. It is molecular weight independent and characterized by an important loss of motional cooperativity with increasing temperature. The T_1 data interpretation is confirmed by the NOEF data which exhibit a leveling off at an abnormally high value (0.9 at 20.1 MHz and 0.8 at 100.6 MHz) with decreasing temperature below about 50 °C. It is shown that such a behavior can be theoretically predicted as a general limit behavior for an excessive dispersion of motional modes in a polymer chain. It is also shown that NOEF is much more discriminating than T_1 for testing model relevancy. Some failures were encountered with the Jones–Stockmayer model, the latter being unable to properly account for either the T_1 or the NOEF data in the regime of excessive dispersion. Also characterized was a temperature-independent correlation time for the methyl group internal rotation in polyisoprene.

Introduction

High-resolution ^{13}C NMR spin relaxation techniques are currently used for studying molecular motion in various polymeric systems including solutions,[1-5] melts,[6] elastomers,[1,7,8] and glassy[9] or semicrystalline solids.[6,10,11] For solutions, melts, and elastomers, spin relaxation parameters of individual ^{13}C nuclei can be measured by means of conventional high-resolution NMR apparatus. Similar studies are possible for glassy and semicrystalline polymers but require NMR apparatus that can provide solid-state high-resolution spectra by means of the so-called magic-angle spinning experiment.[12] Spinning at magic-angle is unnecessary for obtaining high-resolution spectra of bulk elastomers because local motion in such materials is sufficiently rapid to average out the dipolar magnetic interactions between ^{13}C and ^{1}H nuclei. Moreover, conventional NMR studies made on either filled or thermoplastic elastomers may yield line width perturbations that can be interpreted in terms of the hard-phase interaction with the rubbery matrix.[7,13-15]

Among the ^{13}C spin relaxation parameters that can be easily measured with conventional NMR apparatus are the spin–lattice relaxation time, T_1, and the nuclear Overhauser enhancement factor, NOEF. Both these parameters are governed by the spectral density function $J(\omega)$, which characterizes the frequency distribution of the local magnetic field produced by the motion of ^{1}H nuclei in proximity of the ^{13}C nuclei. For a system in which the C–H vectors are undergoing a simple isotropic rotation characterized by a correlation time, τ, $J(\omega)$ is given by the familiar expression:[1]

$$J(\omega) = \tau/(1 + \omega^2\tau^2) \quad (1)$$

For C–H vectors within the backbone of a flexible chain, the main sources of high-frequency motion are bond oscillations and local conformational changes like crankshaft rotations. The combination of these motions might result in nearly isotropic reorientations characterized by more than one correlation time, but there is not definitive proof or argument that this is really the case. On the other hand, rotation of the whole chain or tumbling of large portion of the chain can occur but at much lower frequencies than the backbone local rearrangements. Therefore, it is not surprising that eq 1 is an unreallistic model for representing the actual spectral density function for a flexible polymer chain as it is well documented in the literature.[1-5]

Two very distinct approaches have been used for deriving a spectral density function applicable to flexible polymer chains. One of these approaches is purely phenomenological. It consists to fit the experimental relaxation data by means of a distribution of correlation times, $G(\tau)$.[16] This approach assumes that the rigid-rotor model may be used for describing elementary modes of motion, each of them being characterized by a correlation time, τ. Hence, the spectral density function $J(\omega)$ is obtained by averaging eq 1 over all values of τ by means of $G(\tau)$. Empirical distributions of log τ with two adjustable parameters have been proposed along this line.[1,2,16] They all provide an analytical expression for $J(\omega)$ that can be used for quantifying an average value of τ and the distribution width from the experimental spin relaxation data.[1,2,7,8]

The second approach is based on the research for a relevant molecular model capable of describing the local backbone motions of a flexible chain. This approach is a formidable task, and the most successful results obtained along this line were initiated by Valeur et al.,[17] who developed a model based on conformational jumps articulated on a tetrahedral lattice. This model, as well as an alternative form of it derived by Jones and Stockmayer,[18] also yields two adjustable parameter expressions for $J(\omega)$ that were shown to give acceptable fittings for NMR spin relaxation data of various systems including solutions[2-5,19] and rubbery materials.[19] One of the adjustable parameters is the harmonic average correlation time for the conformational jumps, τ_h, a quantity implicitly defined in the model. In Valeur et al. theory, the second parameter is also a correlation time. It is related to any other existing reorientation processes not taken into account by the conformational jump process, including tumbling of the whole molecule.[5] This second parameter was introduced semiemperically and for that reason has no clear physical meaning. In Jones and Stockmayer theory, the second parameter is not a correlation time. It is a quantity related

0024-9297/89/2222-1307$01.50/0

to the segment length over which bond directional correlations exist.

The aim of the present work was to establish an analytical framework for the ^{13}C relaxation data of polyisoprene that could be used to investigate molecular motion in phase-separated block polymers containing a polyisoprene microphase. For that purpose, T_1 and NOEF of various ^{13}C nuclei in bulk monodisperse polyisoprene samples of very different molecular weights ($M_n = 7 \times 10^3$ and 1.3×10^5) were measured over the temperature interval from 20 to 100 °C at well-separated ^{13}C Larmor frequencies (20.6 and 100.1 MHz). This provided us with a large amount of experimental independent variables that could be used for testing the merits of the foregoing models over a large domain of temperature in which important variations of both T_1 and NOEF were observed. Also observed in the present work was a NOEF leveling off at an abnormally high value with decreasing temperature. It is shown that both the concept of a distribution of correlation times and the conformational jump approach can predict such an effect. For the sake of conciseness, the present analysis is restricted to the use of the χ^2 distribution proposed by Schaefer[1] and the three-bond jump model derived by Jones and Stockmayer.[18] Either of these models allows a clear interpretation of the relaxation data.

Experimental Section

Materials. The two polyisoprene samples were prepared by anionic polymerization by using *sec*-butyllithium as initiator and benzene as solvent. Their number average molecular weights, M_n, were 7.0×10^3 (tonometry in benzene) and 1.30×10^5 (membrane osmometry in toluene), respectively. Their polydispersity indexes, M_w/M_n, characterized by GPC on the basis of a polystyrene calibration curve were 1.05 and 1.07, respectively. Their glass transition temperatures, T_g, determined by DSC at a heating rate of 10 °C/min were −67 and −63 °C, respectively.

^{13}C NMR Measurements. The ^{13}C NMR measurements were carried out at 20.1 and 100.6 MHz with Bruker WP-80 and WH-400 spectrometers, respectively. The neat samples were studied in 10-mm Wilmad (513-IPP) NMR tubes. The polymers were allowed to flow into the bottom of the tubes by heating the latter at 90 °C in an oil bath. Wilmad (5-mm; 528-PP) vacuum-sealed NMR tubes containing a 1:1 mixture of D_2O and ethylene glycol were inserted concentrically in the 10-mm tubes and kept in place by Teflon spacers. This external mixture provided both deuterium lock for field stability and chemical shift reference. The temperature of the probes was controlled by Bruker unit Model B-ST 100/700 calibrated with a copper–constantan digital thermometer. The spectral widths and the digital resolutions were 9 kHz and 1.5 Hz/point for the 20.1-MHz measurements and 14 kHz and 1.7 Hz/point for the 100.6-MHz measurements.

The ^{13}C spin–lattice relaxation times, T_1, were determined under proton scalar decoupling by using the standard inversion–recovery Fourier transform technique (IRFT). The pulse delay times, PD, in the IRTF sequence (π, t, $\pi/2$, AT, PD) were longer than 5 times the longest T_1 among those to be simultaneously determined. The data acquisition times, AT, were constant at 0.67 s for the 20.1-MHz measurements and at 0.59 s for the 100.6-MHz measurements. For each determination, a series of spectra have been measured for at least 10 values of the delay time t in the range $0–1.5T_1$. The individual T_1 values were computed from the inverse of the least-squares slopes of ln ($S_\infty - S_t$) as a function of t. At each temperature, T_1 determinations were made in triplicate with a reproducibility better than about 5%.

The nuclear Overhauser enhancements, NOE, were determined from the intensity ratios of scalar-decoupled and inverse-gated-decoupled spectra. The former where measured with the sequence (PD_1, $\pi/2$, AT) with $PD_1 > 5T_1$ and the latter with the sequence (PD_2 $\pi/2$, AT) with $PD_2 > 10T_1$. In the latter sequence the decoupler was turned off during the pulse delay time PD_2. This yields NOE-suppressed spectra with proton-decoupled singlets. In order to minimize errors resulting from sampling changes, both sequences were run alternatively and their respective FID's were accumulated in different memories of the hardware. At each temperature, NOE determinations were made in triplicate with a reproductibility of about ±0.05. Nuclear Overhauser enhancement factor, NOEF, corresponds to the relative increase of intensity due to Overhauser effect. It is given by the quantity NOE − 1.

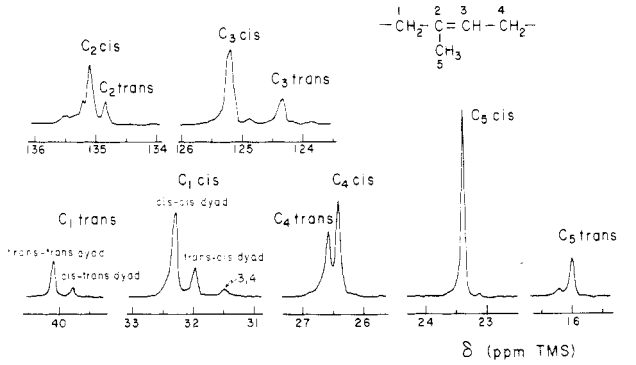

Figure 1. Main segments of 100.6-MHz proton-decoupled ^{13}C NMR spectrum measured at 100 °C for the low molecular weight ($M_n = 7 \times 10^3$) bulk polyisoprene sample. The other resonances not shown in these segments were the ethylene glycol peak at 62.9 ppm and the 3,4 unit tiny peaks at 19.0, 29.9, 111.2, and 148.0 ppm.

Results and Discussion

The experimental T_1 and NOEF data examined are those related to the cis-1,4 units in the present polyisoprene samples. These units contribute to 71% of their microstructure. The relaxation data of the other units, trans-1,4 (22%) and -3,4 (7%), are not examined. The carbon nuclei of the cis-1,4 units are numbered as follows:

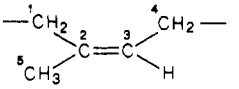

Figure 1 shows a 100.6-MHz proton-decoupled spectrum measured at 100 °C for the low molecular weight material. It may be seen that the C_1 methylene resonances of the cis-1,4 and trans-1,4 units (well separated at 32 and 40 ppm, respectively) exhibit dyad effects. Both are split into pairs of peaks that correspond to C_1 cis carbons in cis–cis and trans–cis dyads and to C_1 trans carbons in trans–trans and cis–trans dyads, respectively. In a previous paper,[20] this feature made it possible to define a random distribution for the cis and trans unit placements in the present materials.

Not only such a sensitivity to dyad environment is not observed for the C_4 cis and trans methylene resonances, but also the latter (observed near 26.5 ppm) are not perfectly resolved even at 100.6 MHz. For that reason, only the methylene relaxation parameters (T_1 and NOEF) of the C_1 cis carbons are analyzed in the present study. From the measurements made at 100.6 MHz, it has been possible to determine that the C_1 cis carbons in cis–cis and trans–cis dyads yield the same values of T_1 and NOEF. The other cis-1,4 unit carbon nuclei whose relaxation parameters are analyzed in the present study are those of the C_3 methine and the C_5 methyl groups. Their resonances appear under the form of single peaks at 125 and 23.5 ppm, respectively. The C_2 carbon was excluded because T_1 interpretation of a unprotonated carbon is not a simple matter. The 20.1-MHz measurements were performed for both the low and high molecular weight samples, while 100.6-MHz measurements were performed on the low molecular weight material only.

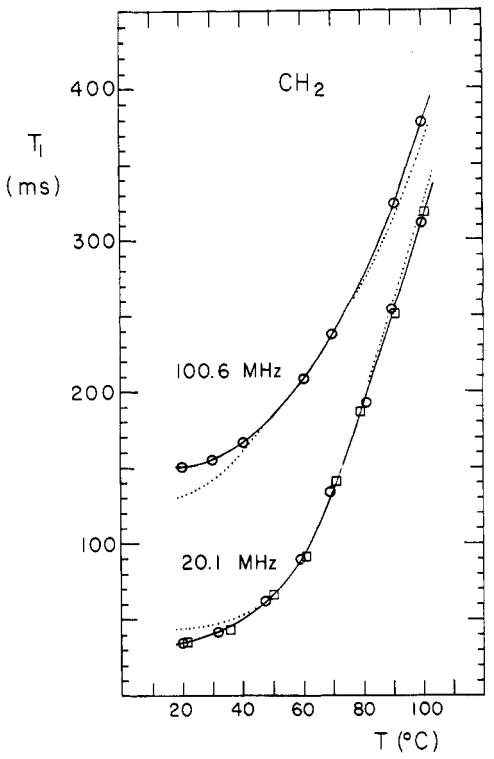

Figure 2. Temperature dependence of T_1 for the methylene C_1 *cis* resonance at 20.1 and 100.6 MHz, respectively. Circle and square data points correspond to the low and high molecular weight samples, respectively. Solid curves correspond to the χ^2 distribution fitting while dotted curves correspond to Jones–Stockmayer model fitting. Parameters for both fittings are listed in Table I.

T_1 Data and Model Parameter Adjustment. Figure 2 shows the methylene carbon T_1 values plotted as a function of temperature in the range from 20 to 100 °C. From the data at 20.1 MHz, it may be seen that T_1 of this carbon does not depend upon molecular weight over the whole range of temperature. This indicates that methylene spin–lattice relaxation in the low molecular weight material is essentially governed by segmental motions. Therefore its independent values measured at 20.1 and 100.6 MHz are well indicated for adjusting the model parameters, namely, those of the χ^2 distribution proposed by Schaefer and those of the Jones–Stockmayer three-bond jump theory. As it may be seen in Figure 2 the T_1 values measured at these two frequencies are well apart and known with a good accuracy. The next step will be to test the models through the NOEF data measured at the same frequencies.

The normalized χ^2 distribution function proposed by Schaefer[1] is written in terms of a variable S which is a b–base logarithmic function of τ

$$F(S) = (1/\Gamma(p))(pS)^{p-1}p \exp(-pS) \quad (2)$$

$$S = \log_b [1 + (b - 1)(\tau/\tau_0)] \quad (3)$$

where τ_0 is the average correlation time corresponding to the mean value of S ($\bar{S} = 1$), p is a width parameter whose inverse corresponds to the variance, σ^2, of the χ^2 distribution, and $\Gamma(p)$ is the γ function of p.

The average value of the spectral density function, $\bar{J}(\omega)$, for a given value of ω can be computed by numerical integration

$$\bar{J}(\omega) = \int_0^\infty [\tau/(1 + \omega^2\tau^2)]G(\tau)\, d\tau \quad (4)$$

with

$$G(\tau)\, d\tau = F(S)\, dS \quad (5)$$

The Jones–Stockmayer theory for segmental motion is based on an elementary three-bond jump process occurring in the center of a segment of finite length containing $2m - 1$ bonds arranged on a tetrahedral lattice. The parameter $2m - 1$ corresponds to a kinetic segment length, that is the bond number over which there is directional correlation between alternate bonds. The second parameter is the harmonic average, τ_h, of the correlation times associated with the $s = (m + 1)/2$ modes of motion within the kinetic segments. This theory yields the following expression for $J(\omega)$[19]

$$J(\omega) = \sum_{k=1}^{s} [G_k\tau_k/(1 + \omega^2\tau_k^2)] \quad (6)$$

with

$$(1/\tau_k) = (2/\tau_h) \sin^2 [(2k - 1)\pi/(2m + 2)] \quad (7)$$

$$G_k = (1/s) + (2/s)\sum_{q=1}^{s-1} \exp(-q \ln 9) \cos [q(2k - 1)\pi/2s] \quad (8)$$

Since the sum of G_k's is unity, the formalism of eq 6 is identical with that of eq 4 for the average of $J(\omega)$ given by a distribution function of τ. The difference between the two results lies in the limited number, s, of discrete values of τ for the Jones–Stockmayer model. Since s corresponds to the quantity $(m + 1)/2$, it is a linear function of the kinetic segment length over which bond motion exhibits cooperativity. On the other hand, it also characterizes the width of the correlation time distribution. By analogy, the quantity $1/p$ of the χ^2 distribution may also be considered as a measure of the extent of the cooperative motion within the chain backbone.

In the case of a purely dipolar relaxation mechanism, eq 4 or eq 6 of either model can be applied to compute the relaxation parameters T_1 and NOEF of a backbone CH_N group by means of the following well-known relationships:[21]

$$T_1^{-1} = Na[3J(\omega_C) + J(\omega_H - \omega_C) + 6J(\omega_H + \omega_C)] \quad (9)$$

$$a = (\mu_0/4\pi)^2(h/2\pi)^2\gamma_C^2\gamma_H^2/10r^6 \quad (10)$$

$$\text{NOEF} = (\gamma_H/\gamma_C)\frac{[6J(\omega_H + \omega_C) - J(\omega_H - \omega_C)]}{[3J(\omega_C) + J(\omega_H - \omega_C) + 6J(\omega_H + \omega_C)]} \quad (11)$$

where γ_C ($6.73 \times 10^7 T^{-1}$ s^{-1}) and γ_H (2.675×10^8 T^{-1} s^{-1}) are the magnetogyric ratios of the ^{13}C and ^1H nuclei, respectively, μ_0 is the vacuum magnetic permeability, h is Planck's constant, and r is the C–H bond length. For r = 0.109 nm, the value generally quoted for CH_2 sp^3 groups, the constant a is equal to 2.15×10^9 s^{-1}.

By using the χ^2 distribution it has been possible to fit the T_1 data in Figure 2 over the whole range of temperature from 20 to 100 C. For that purpose a logarithmic base of 1000 was used in eq 3. The fitting was applied to the smooth curves drawn through the T_1 data at intervals of 10 °C from 20 to 100 °C. The values of the parameters τ_0 and p giving a perfect reproduction of these curves at each temperature are listed in Table I.

Figure 3 shows an Arrhenius plot of τ_0. Above this plot is shown the temperature dependence of the distribution width $1/p$. It may be seen that the Arrhenius plot of τ_0 consists of two linear segments that intersect at a temperature close to 59 °C. The apparent activation energy for the low-temperature segment is 65 kJ mol^{-1} while that for the high-temperature segment is 19 kJ mol^{-1}. It may

Table I
Model Parameters for Segmental Motion Adjusted from the Methylene T_1 Data Measured at 20.1 and 100.6 MHz[a]

T (°C)	τ_0 (ps)	p	τ_h (ps)	$2m-1$	τ_0/τ_h
20	2000	7	250	29	8.0
30	1000	7	200	29	5.0
40	400	8	130	25	3.1
50	170	11	83	25	2.0
60	100	14	45	21	2.2
70	73	24	31.5	17	2.3
80	62	34	25.5	13	2.4
90	53	45	25	9	2.1
100	43	47	20	9	2.2

[a] The quantities τ_0 and p refer to the χ^2 distribution model while the quantities τ_h and $2m-1$ refer to the Jones–Stockmayer model.

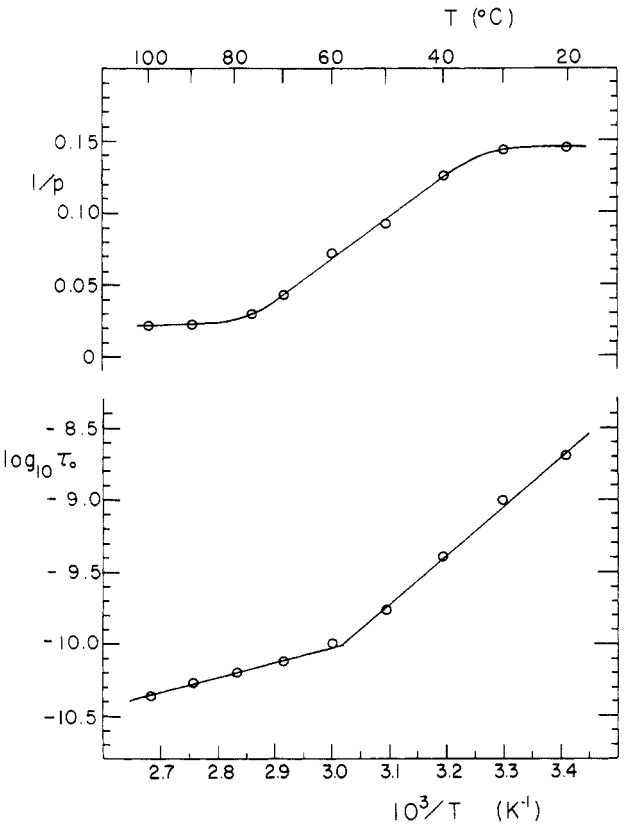

Figure 3. Arrhenius plot of the average correlation time τ_0 for segmental motion obtained by the χ^2 distribution fitting of the methylene T_1 data in Figure 2. Also shown is the temperature dependence of the variance $1/p$ of the χ^2 distribution.

also be seen in Figure 3 that the distribution width, $1/p$, exhibits a sigmoidal increase from the value 0.02 to the value 0.14 with decreasing temperature. It thus appears that the change of regime observed in the Arrhenius plot of τ_0 corresponds to a substantial broadening of the correlation time distribution.

With the Jones–Stockmayer three-bond jump model, that is with eq 6, it has not been possible to obtain a perfect fit of the methylene T_1 data over all the temperature range of the present study. As it may be seen in Figure 2 where the best fit obtainable with this model is described by dotted curves, an important discrepancy occurs in the temperature region below about 40 °C where the model is unable to account for the large difference between the T_1 values measured at 100.6 and 20.1 MHz, respectively.[22] A similar discrepancy is also observed in the region of the high temperatures, but the latter is less important and remains within the experimental error of 5% estimated for the T_1 measurements.

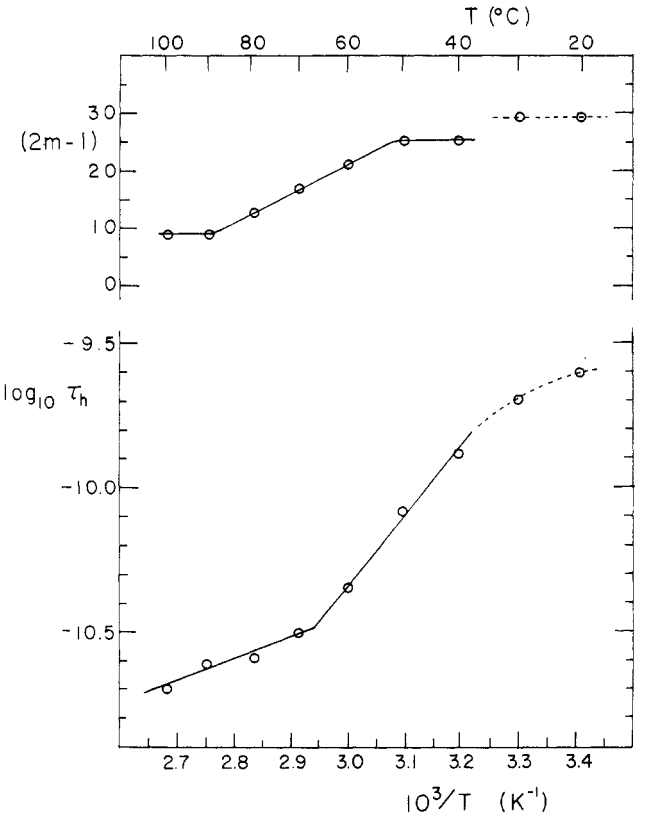

Figure 4. Arrhenius plot of the harmonic average correlation time τ_h for segmental motion obtained by Jones–Stockmayer model fitting of the methylene T_1 data in Figure 2. Also shown is the temperature dependence of the kinetic segment length $2m-1$ for directional correlation. Dashed segments correspond to the temperature range where this model fails to provide a good fit to the T_1 data.

The model parameters τ_h and $2m-1$ corresponding to the dotted curves in Figure 2 are listed in Table I together with the parameters τ_0 and p of the preceding model. Also listed in the last column of Table I are the ratios τ_0/τ_h. It may be seen that the latter are close to the value 2.2 ± 0.2 for all temperatures above 40 °C. In the range from 40 to 20 °C, τ_0/τ_h progressively increases up to the value 8.0 but a substantial part of this increase is probably associated with the observed failure of the Jones–Stockmayer model to predict the T_1 behavior in this temperature range.

Figure 4 shows an Arrhenius plot of τ_h above which is depicted the temperature dependence of the correlation length parameter $2m-1$. As expected from the constancy of the ratios τ_0/τ_h in Table I, a discontinuity is also observed in the Arrhenius plot of τ_h. It occurs at 66 °C, a temperature slightly above that (59 °C) observed in the Arrhenius plot of τ_0. The apparent activation energy computed from the high-temperature segment of τ_h is 15 kJ/mol (compared to 19 kJ/mol for τ_0) while that of the low-temperature segment is 47 kJ/mol (compared to 65 kJ/mol for τ_0). Also, as for the preceding model, the change of regime for τ_h corresponds to a sigmoidal increase of the orientational correlation length, $2m-1$, with decreasing temperature. According to the difference between the foregoing activation energies for the low- and high-temperature segments in the Arrhenius plot of Figure 4, this change in the $2m-1$ curve may be interpreted as the consequence of a potential barrier of about 30 kJ/mol that would produce an important increase of the coupling extent between segmental motions in the polymer chains. Indeed, on the basis of the straightforward physical meaning of the parameter $2m-1$ of the present model,

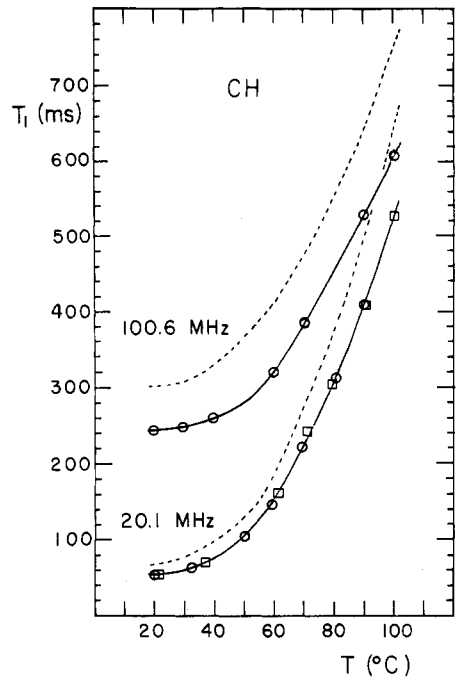

Figure 5. Temperature dependence of T_1 for the methine C_3 cis resonance at 20.1 and 100.6 MHz, respectively. Circle and square data points correspond to the low and high molecular weight samples, respectively. The dashed curves shows the T_1 methine values predicted on the basis of the methylene T_1 data in Figure 2 by assuming same segmental motion, same C–H bond length, and absence of nondirectly bonded proton effect for both groups.

the average number of virtual bonds in the kinetic segments would increase from 9 to 25 with decreasing temperature from 90 to 50 °C with a leveling off at both ends of this temperature range.

The experimental T_1 data concerning the methine backbone carbon are depicted in Figure 5 where it may be seen that, like the methylene data, they are molecular weight independent over the whole range of temperature. Figure 5 also shows the methine T_1 values (dashed curves) expected on the basis of the corresponding methylene T_1 values depicted in Figure 2. Indeed, on the ground of eq 9 derived for a purely dipolar relaxation mechanism, the former should be twice as large as the latter. Such a model-independent prediction assumes that the C–H internuclear vector motions in either group are governed by the same segmental motions. Furthermore, it assumes that the C–H bond length in either group is the same and also that the nondirectly bonded protons have a negligible contribution to T_1 of either group.

It may be seen in Figure 5 that the expected methine T_1 values are greater than the experimental values by a frequency independent constant factor close to 1.24. This immediately suggests that either one or both of the last assumptions should be revised. In fact, a C–H bond length in the methine group shorter by 3.6% with respect to that in the methylene group would be sufficient to account for the observed discrepancy. On the other hand, it is likely that the protons on the neighboring methylene and methyl groups are contributing to a fraction of the observed reduction of T_1 for this one-proton bearing carbon. Therefore, the methine T_1 data in Figure 5 are not inconsistent with a purely dipolar relaxation mechanism. This, together with the fact that the above discrepancy is of constant magnitude (24%) over the whole temperature range of the present study, suggests that the coplanar vinyl groups in the present polyisoprene are entities undergoing spatial reorientation correlated with that of the neighboring methylene groups. This will be confirmed shortly in the next T_1 analysis addressed to the methyl group motions.

The C–H vector reorientation for a methyl group attached to a polymer chain is modulated by both the internal rotation of the group around its symmetry axis and the overall motion of the backbone segment on which this group is bonded. In the present case, the latter can be assumed to be characterized by either one of the parameter pairs, τ_0, p or τ_h, $2m - 1$, listed in Table I.

Both the χ^2 distribution approach and the Jones–Stockmayer model for segmental motion can be easily generalized to the case of an internally rotating group by means of a third parameter, τ_{rot}, characterizing the correlation time for the rotational motion. The basis for such a generalization can be found in Woessner theory[23] for a spin system undergoing internal rotation within a molecule submitted to overall isotropic reorientation. It yields a modification of eq 1 for $J(\omega)$ that can be applied directly in either eq 4 or eq 6 of the present models. If one defines by θ the angle beween the C–H vector and the axis of internal rotation (109.47° for a methyl group), this modification is[23]

$$J(\omega) = A\frac{\tau}{(1 + \omega^2\tau^2)} + B\frac{\tau_B}{(1 + \omega^2\tau_B^2)} + C\frac{\tau_C}{(1 + \omega^2\tau_C^2)} \tag{12}$$

where

$$A = (1/4)(3\cos^2\theta - 1)^2 \tag{13}$$

$$B = (3/4)\sin^2 2\theta \tag{14}$$

$$C = (3/4)\sin^4\theta \tag{15}$$

$$(1/\tau_B) = (1/\tau) + (1/\tau_{rot}) \tag{16}$$

$$(1/\tau_C) = (1/\tau) + (4/\tau_{rot}) \tag{17}$$

Equations 16 and 17 hold for a simple rotation not modulated by potential barriers. In the case of a methyl group, a more realistic model is a random jump through three equivalent orientations 120° apart from each other. For that particular case, Woessner derived the following relation for τ_B and τ_C.[23]

$$(1/\tau_B) = (1/\tau_C) = (1/\tau) + (1/\tau_{rot}) \tag{18}$$

In eq 16–18 τ is the correlation time for the reorientation of the axis of rotation, that is for the overall motion of the methyl group bearing entity. If, as mentioned previously, one assumes that this latter motion has been properly characterized by the foregoing analysis of the methylene T_1 data, eq 12 together with eq 18 can be used to fit the methyl T_1 data by adjusting τ_{rot} only. For the χ^2 distribution model, the computation necessary for this fitting involves a numerical integration of eq 4 after substitution of eq 12 into it. For the Jones–Stockmayer three-bond jump model, the computation is made from eq 6 after substitution of the three terms of eq 12 into it.[18]

The T_1 methyl data are shown in Figure 6 together with the best fittings made with both the χ^2 distribution model (full curves) and the Jones–Stockmayer model (dotted curves). In each case, the best fitting was obtained by adjusting τ_{rot} to the same value throughout the temperature range of the present study. This τ_{rot} value is 3×10^{-13} s for the χ^2 model and 1×10^{-13} s for the Jones–Stockmayer model. The difference is rather small if one considers either that the models involve a nonnegligible contribution of segmental motion to the T_1 values and that this con-

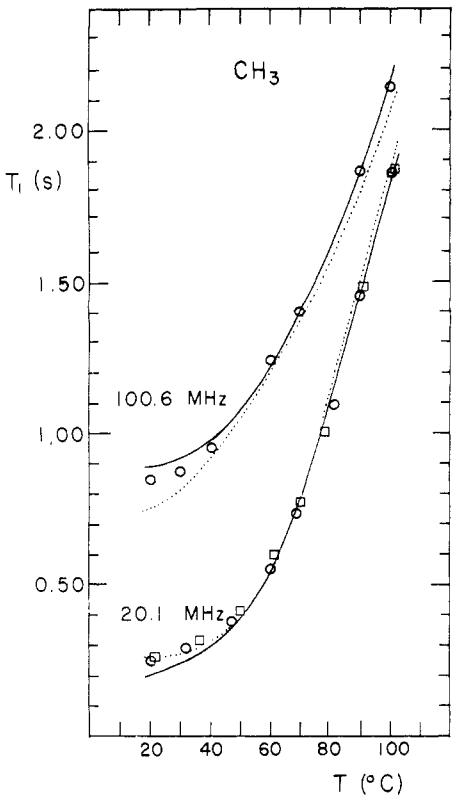

Figure 6. Temperature dependence of T_1 for the methyl C_5 cis resonance at 20.1 and 100.6 MHz, respectively. Circle and square data points correspond to the low and high molecular weight samples, respectively. Solid curves correspond to χ^2 distribution fitting with $\tau_{rot} = 3 \times 10^{-13}$ s while dotted curves correspond to Jones–Stockmayer model fitting with $\tau_{rot} = 1 \times 10^{-13}$ s. Both fittings are based on the model parameters for segmental motion listed in Table I.

tribution is taken into account by very different approaches.

Inspection of Figure 6 shows that both models provide an excellent fitting of the 20.1- and 100.6-MHz T_1 data in the temperature range above 40 °C. Below this temperature, only a change in the parameters τ_0 and p of the χ^2 distribution could have provided a better fitting at the two frequencies. An increase of τ_{rot} would have contributed to decrease both the 20.1- and 100.6-MHz T_1 while a decrease of τ_{rot} would have contributed to increase the 100.6-MHz T_1 without a significative change for the 20.1-MHz T_1. Turning to the Jones–Stockmayer model, it may be seen in Figure 6 that it provides a better fitting than the χ^2 distribution for the 20.1-MHz T_1 data in the temperature range below 40 °C. Nevertheless, this latter agreement is fallacious since it corresponds to the region where this model failed to provide a good fitting of the methylene T_1 data in the preceding analysis. Indeed, a comparison of Figure 6 with Figure 2 shows that the mismatching features observed between the two models in the case of the methylene T_1 analysis remain present in the background of the present analysis.

The methyl τ_{rot} values in the range $(1–3) \times 10^{-13}$ s inferred from the present analysis fall on the side of the shortest rotational correlation times reported in the literature for methyl rotation in small molecules.[24] This together with the apparent independence of τ_{rot} upon temperature indicates a substantially low barrier to rotation for the methyl group in bulk polyisoprene. Such a feature is apparently due to the coplanarity of the vinyl group that imposes a bond angle of 120° between the methyl and methylene substituents on the C_2 carbon of the polyisoprene unit. This contributes to a substantial lowering of the barrier to rotation of both these substituents with respect to saturated structures.

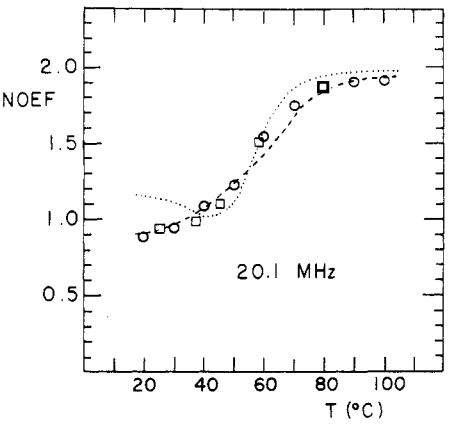

Figure 7. Temperature dependence of NOEF measured at 20.1 MHz for the low (circles) and high (squares) molecular weight samples. Each data point corresponds to the mean value obtained for the methine, methylene, and methyl groups. Individual NOEF values of the latter differ by less than 0.05 (see text). Dashed curve corresponds to NOEF variation predicted by means of the χ^2 distribution parameters in Table I. Dotted curve corresponds to NOEF variation predicted by means of the Jones–Stockmayer model parameters in Table I.

The low T_g of polyisoprene (−67 and −63 °C for the present low and high molecular weight samples, respectively) is certainly a direct consequence of the low barrier to rotation of the methylene substituents on chain flexibility. Curiously, this effect appears to be important enough for counterbalancing the stiffness resulting from the presence of the rigid vinyl groups that account for it. Indeed, complete hydrogenation of polyisoprene having the same microstructure than the present materials produces a minute change of T_g (an increase of 4 °C, only),[25] indicating that the presence of one more flexible bond per monomer unit in the saturated structure has about the same effect on chain flexibility than that provided by the decrease of barrier to rotation due to the coplanarity of the vinyl group in the unsaturated structure.

NOEF Data and Model Predictions. As mentioned at the beginning of the T_1 data analysis, the crucial test for the present models shall be found in their capability to predict some independent relaxation data not previously used for adjusting the model parameters. On the other hand, it is desirable that these data be also exhibiting a good sensitivity to the experimental conditions of temperature and frequency. As it may be seen in Figures 7 and 8, this is precisely the case for the NOEF data measured on the present materials. At both frequencies, the change of NOEF with temperature in the range 20–100 °C is about 20 times larger than the accuracy of ±0.05 estimated for the individual NOEF measurements. Note that within this limit of accuracy NOEF appeared to be invariant with respect to the three carbon nuclei (methine, methylene, and methyl) submitted to the foregoing T_1 analysis. Therefore, the data in Figures 7 and 8 refer to the mean NOEF values measured for the three nuclei at 20.1 and 100.6 MHz, respectively. As it will be shown shortly, this invariance of NOEF among the three nuclei is in good agreement with the model predictions. As for the T_1 data, only the low molecular weight sample has been investigated at 100.6 MHz.

From the 20.1-MHz experimental data in Figure 7 it may be seen that NOEF is molecular weight independent over the whole range of temperature. Also, it may be seen that the 20.1-MHz NOEF values in Figure 7 are systematically

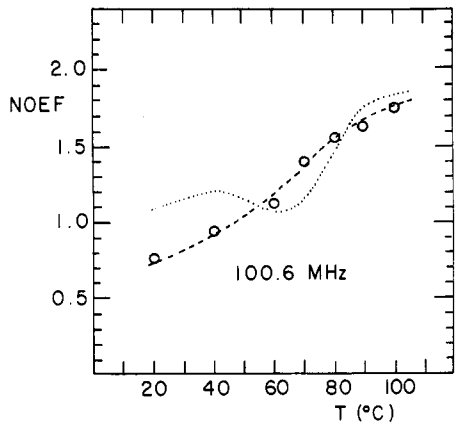

Figure 8. Temperature dependence of NOEF measured at 100.6 MHz for the low molecular weight sample. For curve identification and details see the legend of Figure 7.

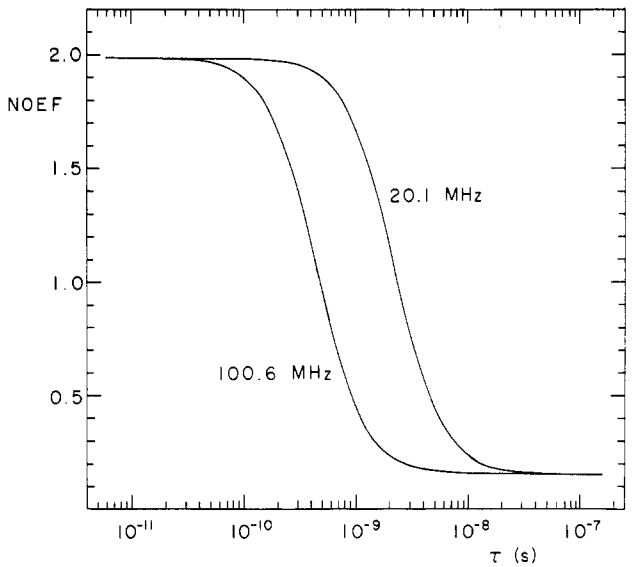

Figure 9. Effect of Larmor frequency upon the correlation time dependence of NOEF in the case of the rigid-rotor model. Theoretical curves computed by means of eq 1 and 11 for the two frequencies (20.1 and 100.6 MHz) used in the present work.

greater than the 100.6-MHz NOEF values in Figure 8. In fact, such a behavior is expected on the basis of the single correlation time model in the region where T_1 exhibits its minimum value. But, contrary to this latter model which, as shown in Figure 9, predicts a sigmoidal decrease of NOEF down to a frequency-independent limit value of 0.153 at long correlation times (low temperatures), the present 20.1-MHz NOEF data exhibit a leveling off at a considerably higher value close to 0.9 with decreasing temperature. For the 100.6-MHz NOEF data the leveling off is less pronounced but is still perceptible in the low-temperature regime.

The theoretical curves presented in Figures 7 and 8 were computed for the methylene resonance on the basis of the model parameters listed in Table I. The dashed curves correspond to the χ^2 distribution model while the dotted curves correspond to the Jones–Stockmayer model. These theoretical curves were obtained by means of eq 11 in which were substituted the appropriate values of $J(\omega)$ computed by using either eq 2–5 for the χ^2 distribution or eq 6–8 for the Jones–Stockmayer model. Similar computations were made for the methyl resonance by taking into account the internal rotation of the methyl group. For that purpose, the appropriate modifications of eq 4 or 6 based upon Woessner eq 12–15 and 18 were used together

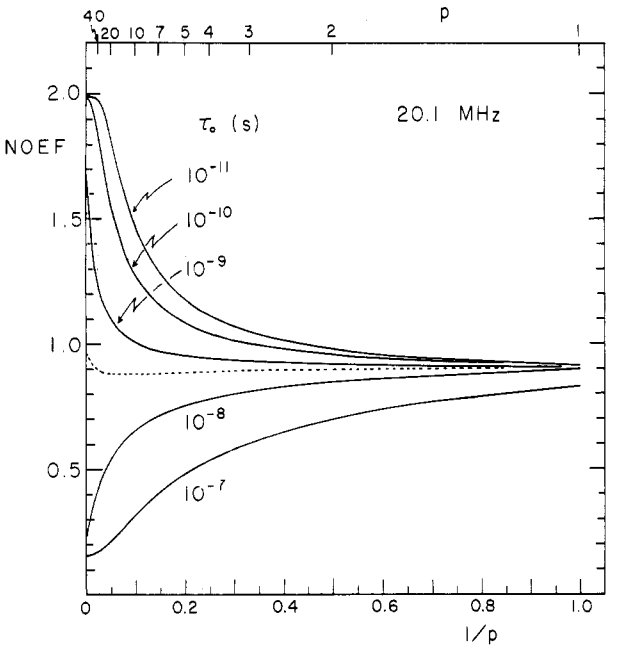

Figure 10. Theoretical dependence of NOEF upon the χ^2 correlation time distribution width $1/p$ showing the asymptotic behavior predicted in the limit of a very broad distribution ($1/p \rightarrow 1$). Curves computed by means of eq 2–5 and 11 as a function of the variance $1/p$ of the χ^2 distribution for different values of the average correlation time τ_0 in the range from 1×10^{-7} to 1×10^{-11} s. Dashed curve corresponds to $\tau_0 = 2.4 \times 10^{-9}$ s.

with the τ_{rot} values (3×10^{-13} s for the χ^2 distribution and 1×10^{-13} s for the Jones–Stockmayer model) determined in the preceding section. This yielded methyl NOEF values slightly greater than the methylene NOEF values. However, even in the best case (that is for the Jones–Stockmayer model at 100.6 MHz) the predicted increase of NOEF due to methyl rotation (in the range 0.01–0.04) was less than the experimental accuracy of ±0.05 estimated for the present measurements.

In both Figures 7 and 8 it may be seen that the predictions based upon the χ^2 distribution (dashed curves) are excellent at either frequency and over all the temperature range of the present study. In fact, the low-temperature leveling off for NOEF at values well above the value of 0.153 predicted by the single correlation time model is a genuine feature associated with the broadening of the correlation time distribution with decreasing temperature. Indeed, as illustrated in Figure 10 for different values of τ_0 in the range from 10^{-7} to 10^{-11} s, the χ^2 distribution model predicts that NOEF measured at 20.1 MHz should either decrease or increase monotically toward a τ_0 independent limiting value close to 0.9 with increasing distribution width $1/p$ toward unity. This limiting behavior should also apply to any other Larmor frequency ω since, as one can see from eq 11, NOEF depends upon a simple ratio of $J(\omega)$'s, that is only on the single variable $\omega\tau_0$. In other words, the 20.1-MHz NOEF theoretical curves depicted in Figure 10 can be applied to 100.6 MHz by simply changing the τ_0 values quoted in this figure by the values $\tau_0/5$.

According to Table I, the largest values of the χ^2 distribution parameters τ_0 and $1/p$ inferred from the foregoing T_1 analysis are 2×10^{-9} s and 0.14, respectively. They are those fitting the methylene data measured at 20 °C. Inspection of Figure 10 shows that for $1/p = 0.14$ the predicted NOEF is still τ_0 dependent. In other words, the limiting behavior (NOEF = 0.9) for very broad distribution ($1/p \rightarrow 1$) is not reached for the present value of $1/p$.

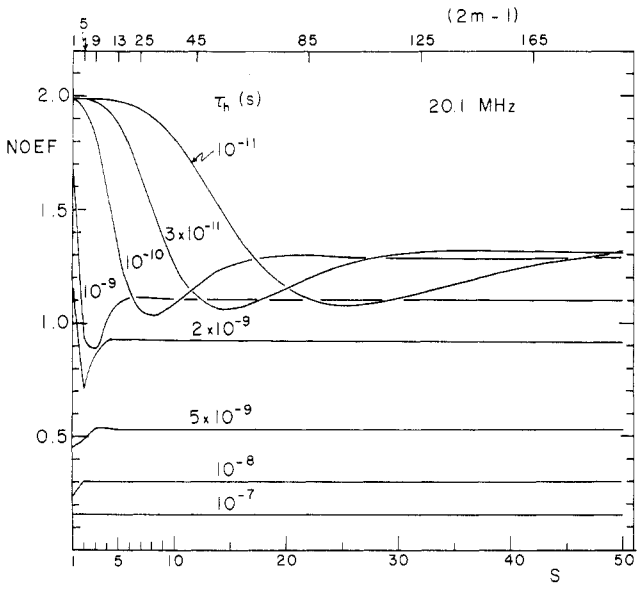

Figure 11. Theoretical dependence of NOEF upon the directional correlation length parameter $2m - 1$ of the Jones–Stockmayer three-bond jump model for segmental motion. Curves computed by means of eq 6–8 and 11 for different values of the harmonic average correlation time τ_h in the range from 1×10^{-7} to 1×10^{-11} s.

Nevertheless, as one can see in Figure 10, the variation of NOEF with τ_0 for $1/p = 0.14$ is restricted to a narrow domain with respect to that allowed by the single correlation time model. For instance, NOEF increases from 0.7 to 1.2 with decreasing τ_0 from 10^{-8} to 10^{-10} s. In the same range of τ_0, the single correlation time model (Figure 9 or the case $1/p = 0$ in Figure 10) predicts an increase of NOEF from the value of 0.24 to the value 1.98. This comparison shows the dramatic reduction of the NOEF domain produced by the broadening of the correlation time distribution. Inspection of Figure 10 also shows that there is a discrete domain of τ_0 for which NOEF converges rapidly toward its theoretical limit. For the 20.1-MHz Lamor frequency this domain is centered around the value $\tau_0 = 2.4 \times 10^{-9}$ s. Therefore, the fact that the 20-MHz NOEF value measured at 20 °C perfectly coincides with the theoretical limit of 0.9 is partly due to a casual effect resulting from the actual τ_0 value (2×10^{-9} s) of the present materials at this temperature.

Turning to the Jones–Stockmayer model, it may be seen in Figures 7 and 8 that this model generates a singularity that is not observed experimentally. Though the NOEF curves predicted by Jones–Stockmayer model (dotted curves in Figure 7 and 8) are globally sigmoidal in shape, they both exhibit a dip prior to their sigmoidal increase. In some way, this feature must be correlated with the previously observed incapability for this model to provide a good fitting of the T_1 data in the temperature range below 40 °C. In fact, above this range, one can observe a good agreement between the predicted and measured NOEF values at 20.1 MHz only (Figure 7). At 100.6 MHz (Figure 8) not only the discrepancy observed at low temperatures is considerably more accentuated than at 20.1 MHz, but also the sigmoidal increase is shifted toward higher temperatures with respect to the experimental data.

Contrary to what was inferred from the foregoing analysis of the χ^2 distribution model, the apparent leveling off at NOEF values near 1.1 that one can observe at low temperatures in the dotted curves of Figures 7 and 8 is not associated with a τ_h-independent limiting behavior for large values of the directional correlation length, $2m - 1$, of the present model. Indeed, as shown in Figure 11 for different values of τ_h in the range from 10^{-7} to 10^{-11} s, the Jones–Stockmayer model yields 20.1-MHz NOEF curves as a function of $2m - 1$ exhibiting limiting asymptotic values that decrease to the single correlation time limit of 0.153 with increasing τ_h. It may also be seen in Figure 11 that the variation of NOEF with $2m - 1$ exhibits a minimum that shifts toward higher $2m - 1$ values with decreasing τ_h. The actual range of τ_h obtained for the present materials lies between 2.5×10^{-10} s at 20 °C and 2×10^{-11} s at 100 °C (Table I). Inspection of Figure 11 shows that all the 20.1-MHz NOEF solutions for this range of τ_h in agreement with the experimental results (those for $T >$ 40 °C in Figure 7) lie on the left side of the NOEF minimum on each curve. On the other hand, the NOEF solutions for $T < 40$ °C at 20.1 MHz, as well as those for $T < 70$ °C at 100.6 MHz (Figure 8), lie on the right side of the NOEF minimum on the NOEF versus $2m - 1$ curves of Figure 11. Note that none of these latter solutions are in agreement with the experimental NOEF data. Thus, as far as the NOEF behavior is concerned, it appears that the Jones–Stockmayer model is severely restricted to situations that can be fitted by the initial decreasing regime observed on the theoretical curves in Figure 11. A similar drawback was encountered when this model was unable to properly fit the methylene T_1 data at $T < 40$ °C.

The NOEF limiting behavior at a value close to 0.9 predicted for very large distributions of correlation times is not a particularity associated with the χ^2 distribution function used for the present analysis. It is a general feature that holds for any other distribution function of $\log \tau$. For instance, as shown in Figure 12, a similar result can be predicted by means of the Cole–Cole distribution function. Contrary to the χ^2 distribution which exhibits a positive skewness, the Cole–Cole distribution is symmetrical.[2,16] When normalized and expressed in terms of a variable S being a linear function of $\ln \tau$, the latter has the form[16]

$$F(S) = (1/2\pi) \sin \gamma\pi/(\cosh \gamma S + \cos \gamma\pi) \quad (19)$$

$$S = \ln (\tau/\tau_0) \quad (20)$$

where τ_0 is the average correlation time corresponding to the mean value of S ($\bar{S} = 0$) and γ is a width parameter whose inverse is an increasing function of the distribution width. The relation between the variance σ^2 of the distribution and this latter parameter is

$$\sigma^2 = (\pi^2/2\gamma) \tan (1 - \gamma)\pi/2 \quad (21)$$

As it may be seen in Figure 12 concerning the variation of NOEF with $1/\gamma$, the main difference issued from the Cole–Cole distribution with respect to the χ^2 distribution, is the prediction of a NOEF leveling off at a value of 0.76 instead of 0.9 for large values of $1/\gamma$. Another difference presumably related to the absence of skewness in the Cole–Cole distribution is the convergence toward exactly the same limiting value (0.76) for all the curve in Figure 12. For the χ^2 distribution the corresponding curves in Figure 10 do not exhibit a perfect convergence.

When Cole–Cole distribution function is used in eq 4 and 5, it yields the following expression for the average of $J(\omega)$:[16]

$$\bar{J}(\omega) = (1/2\omega) \frac{\cos (1 - \gamma)\pi/2}{\cosh (\gamma \ln \omega\tau_0) + \sin (1 - \gamma)\pi/2} \quad (22)$$

Table II shows the parameters τ_0 and γ that give a perfect fit to the methylene T_1 data in Figure 2. Also shown in this table are the ratios $\tau_0(\text{Cole–Cole})/\tau_0(\chi^2)$ and

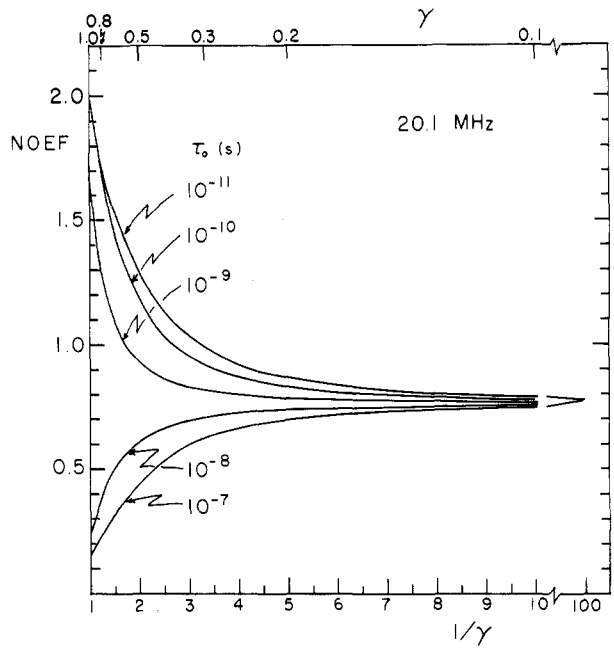

Figure 12. Theoretical dependence of NOEF upon the distribution width parameter $1/\gamma$ of the Cole–Cole distribution. Curves computed by means of eq 22 and 11 for different values of the average correlation time τ_0 in the range from 1×10^{-7} to 1×10^{-11} s.

Table II
Cole–Cole Distribution Parameters for Segmental Motion, τ_0 and γ, Adjusted from the Methylene T_1 Data[a]

T (°C)	τ_0(Cole–Cole) (ps)	γ	τ_0(Cole–Cole)/$\tau_0(\chi^2)$	σ(Cole–Cole/$\sigma(\chi^2)$
20	1300	0.53	0.65	7.7
30	650	0.53	0.65	7.7
40	300	0.53	0.75	8.2
50	155	0.57	0.91	8.7
60	100	0.64	1.00	8.2
70	79	0.76	1.08	7.8
80	70	0.84	1.13	7.1
90	63.5	0.90	1.20	6.2
100	54	0.92	1.25	5.7

[a] Ratios of the correlation times τ_0 and ratios of the standard deviations σ of the variables S defined by eq 20 and 3 for the Cole–Cole and χ^2 distributions, respectively.

σ(Cole–Cole)/$\sigma(\chi^2)$. It may be seen that the former are monotically increasing from 0.65 to 1.25 with increasing temperature from 20 to 100 °C while the latter are about constant at 7.5 ± 1.5 over all this temperature range. Interestingly, this latter result is in close agreement with the value 6.9 obtained for $b = 1000$ according to the following formula

$$\sigma(\text{Cole–Cole})/\sigma(\chi^2) = \ln b \qquad (23)$$

one can derive for the ratio of the standard deviations of the variable S in the χ^2 and Cole–Cole distributions by taking into account the different logarithmic scales of τ used for defining this variable in eq 20 and 3, respectively. Note that an Arrhenius plot of the τ_0 values in Table II also exhibits a change of regime near 60° characterized by low- and high-temperature activation energies intermediate to those inferred from the preceding analyses made with the χ^2 distribution and the Jones–Stockmayer model. In fact, according to the temperature dependence of either p in Table I or γ in Table II, this change of regime for segmental motion would roughly correspond to a decrease by a factor of 2.6 of the standard deviation of ln τ with increasing temperature.

The Cole–Cole distribution parameters in Table II yield about the same values for NOEF as those computed from the χ^2 distribution (dashed curves in Figures 7 and 8). In all cases the difference is less than 0.1 NOEF unit. Also, when applied to the fitting of the methyl T_1 data in Figure 6, these parameters yield a temperature-independent τ_{rot} value of 1×10^{-13} for the methyl rotation, a result in good agreement with the foregoing values of 3×10^{-13} and 1×10^{-13} s obtained with the χ^2 distribution and the Jones–Stockmayer model, respectively. So, at first glance, there is no particular advantage in taking a distribution with positive skewness, like the χ^2 distribution, for analysing either T_1 or NOEF data.

Conclusion

According to the T_1 and NOEF data measured at 20.1 MHz for the present low and high molecular weight polyisoprene samples, segmental motion in bulk polyisoprene appears to be molecular weight independent down to molecular weights as low as 7×10^3. This is not surprising since the T_g measured by DSC for the sample having this low molecular weight exhibits a minute depression of only 4 °C with respect to the T_g of its high molecular weight homologue.

The main feature concerning polyisoprene segmental motion is its change of regime near 60 °C. Unambiguous evidence for this transition appears in the Arrhenius plots of the average correlation times (τ_0 or τ_h) determined from the methylene T_1 data on the basis of the two different models. This change of regime is characterized by an important loss of motional cooperativity evidenced by a sigmoidal decrease in the number of segmental motion modes with increasing temperature. In terms of the distribution approach this change is quantified by a drop by a factor of about 2.6 in the standard deviation of ln τ, while in terms of the Jones–Stockmayer model it corresponds to a threefold decrease in the kinetic segment length for orientational correlation. Roughly, a concomitant threefold decrease is also observed in the apparent activation energy for segmental motion. Above about 60 °C, depending upon the models, the latter decreases to values in the range 15–19 kJ/mol compared to values in the range 47–65 kJ/mol for the low-temperature regime. The values for the high-temperature regime appear to be in the range of those previously obtained for segmental motion of various polymers in 10% solutions.[2-5]

These features concerning the dynamics of the polyisoprene backbone are apparently not artifacts resulting from the present model fittings of the methylene T_1 data. Evidence that they are genuine features clearly appears in the NOEF variation with temperature. Indeed, below about 50 °C the latter exhibits a leveling off at an abnormally high value that cannot be explained without considering a change of regime for the backbone motion. In other words, contrary to T_1 studies, NOEF studies as a function of temperature can provide direct experimental evidence whenever a large dispersion of the C–H vector motion frequencies occurs in a polymer system. It also appears that NOEF is a much more discriminating physical quantity than T_1 for testing model relevancy. On the basis of the present analysis, there is no doubt that the distribution approach is more coherent than the three-bond jump model concerning NOEF behavior. In fact, only the former can predict as a general behavior a leveling off for NOEF at a value in the range 0.8–0.9 in the limit of a very large number of motional modes for the backbone segments.

The problem inherent with the Jones–Stockmayer model is thus well identified. It consists in its incapability to

properly account for the relaxation behavior when excessive dispersion of motional modes is encountered. This was observed for both T_1 and NOEF at temperatures below about 40 °C in the present work. Nevertheless, for moderate dispersions this model appears to provide coherent predictions and founded interpretations. In fact, the problem encountered for the low-temperature data in the present work did not shadow any of the foregoing features concerning the polyisoprene backbone dynamics as well as those concerning the methyl group motion in this polymer. Well on the contrary, Jones–Stockmayer model has provided a strong confirmation of any of these features together with a possibility for their interpretation on a molecular basis in terms of a kinetic segment length for cooperative motion.

Acknowledgment. This work was supported by National Sciences and Engineering Council of Canada and the Quebec Ministry of Education. We thank Dr. M. T. Pham Viet and Mr. R. Mayer of this Department for their advice and help for the NMR measurements.

Registry No. Polyisoprene, 9003-31-0.

References and Notes

(1) Schaefer, J. *Macromolecules* **1973**, *6*, 882.
(2) Heatley, F.; Begum, A. *Polymer* **1976**, *17*, 339.
(3) Schilling, F. C.; Cais, R. E.; Bovey, F. A. *Macromolecules* **1978**, *11*, 325.
(4) Jones, A. A.; Bisceglia, M. *Macromolecules* **1979**, *12*, 1136.
(5) Têkêli, P.; Lauprêtre, F.; Monnerie, L. *Macromolecules* **1983**, *16*, 415.
(6) Axelson, D. E.; Mandelkern, L. *ACS Symp. Ser.* **1979**, *No. 103*, 181.
(7) Komoroski, R. A.; Maxfield, J.; Mandelkern, L. *Macromolecules* **1977**, *10*, 545.
(8) Dekmezian, A.; Axelson, D. E.; Detchter, J. J.; Borah, B.; Mandelkern, L. *J. Polym. Sci., Polym. Phys. Ed.* **1985**, *23*, 367.
(9) Schaefer, J.; Sefcik, M. D.; Stejskal, E. O.; McKay, R. A.; Dixon, W. T.; Cais, R. E. *Macromolecules* **1984**, *17*, 1107.
(10) Stefcik, M. D.; Schaefer, J.; Stejskal, E. O.; McKay, R. A.; *Macromolecules* **1980**, *13*, 1132.
(11) Jelinski, L. W.; Dumais, J. J.; Engel, A. K. *Macromolecules* **1983**, *16*, 403.
(12) Axelson, D. E.; Russell, K. E. *Prog. Polym. Sci.* **1985**, *11*, 221.
(13) Schaefer, J. *Macromolecules* **1972**, *5*, 427.
(14) Morêse-Séguêla, B.; St-Jacques, M.; Renaud, J. M.; Prud'homme, J. *Macromolecules* **1980**, *13*, 100.
(15) Jelinski, L. W.; Schilling, F. C.; Bovey, F. A. *Macromolecules* **1981**, *14*, 581.
(16) Connor, T. M. *Trans. Faraday Soc.* **1964**, *60*, 1574.
(17) Valeur, B.; Jarry, J. P.; Geny, F.; Monnerie, L. *J. Polym. Sci., Polym. Phys. Ed.* **1975**, *13*, 667, 675, 2251.
(18) Jones, A. A.; Stockmayer, W. H. *J. Polym. Sci., Polym. Phys. Ed.* **1977**, *15*, 847.
(19) Jones, A. A.; Robinson, G. L.; Gerr, F. E. *ACS Symp. Ser.* **1979**, *No. 103*, 271.
(20) Morêse-Séguêla, B.; St-Jacques, M.; Renaud, J. M.; Prud'homme, J. *Macromolecules* **1977**, *10*, 431.
(21) Doddrell, D.; Glushko, V.; Allerhand, A. *J. Chem. Phys.* **1972**, *56*, 3683.
(22) **Note Added in Proof.** Since this manuscript was submitted, there has been a series of three papers by Dejean de la Batie, Lauprêtre, and Monnerie accepted for publication in this journal that propose a solution for tackling this problem. In these papers, a clever modification to the conformational jump model is derived by taking into consideration local anisotropic motions described by a fast libration of the C–H vectors in addition to segmental motion. This modification yields a four-parameter equation for T_1 that can be adjusted to properly fit the T_1 minima for many elastomers including polyisoprene. As we could see in the last of these papers whose manuscript was kindly sent to us by Dr. Bovey for the review purpose of this paper, such a fitting for the T_1 minima is unfortunately made to the detriment of a good fitting for the T_1 data over a wide range of temperature above the T_1 minima. This suggests that the correlation time distribution concept still remains the most efficient approach for taking into account the excessively wide spectrum of rapid motions that appears to be a characteristic of many elastomers at temperatures below about T_g + 80 °C.
(23) Woessner, D. E.; Snowden, B. S.; Meyer, J. H. *J. Chem. Phys.* **1969**, *50*, 719.
(24) Wehrli, F. W.; Wirthlin, T. *Interpretation of Carbon-13 NMR Spectra*; Heyden: New York, 1976; p 252.
(25) Laramée, A.; Goursot, P.; Prud'homme, J. *Makromol. Chem.* **1975**, *176*, 3079.